Applied Energy 107 (2013) 25–32

Contents lists available at SciVerse ScienceDirect

Applied Energy

journal homepage: www.elsevier.com/locate/apenergy

Configuration effects of natural gas fired multi-pair regenerative burners in a flameless oxidation furnace on efficiency and emissions

E.-S. Cho [a], D. Shin [a,b,*], J. Lu [a], W. de Jong [a], D.J.E.M. Roekaerts [a]

[a] Process & Energy, 3mE, Delft University of Technology, The Netherlands
[b] School of Mechanical Engineering, Kookmin University, South Korea

HIGHLIGHTS

- We executed experiments and simulations for flameless oxidation burner.
- Four combinations of burner were examined to derive out reaction characteristics.
- Single digit of NO and CO occurred together for a parallel burner configuration.
- Smooke reaction model shows reasonable explanation of flameless oxidation.
- However, the reaction kinetics is lower than the experimental results.

ARTICLE INFO

Article history:
Received 25 June 2012
Received in revised form 8 January 2013
Accepted 15 January 2013
Available online 6 March 2013

Keywords:
Flameless oxidation
Regenerative burner
Burner configuration
Cycle time
CO emission
NO emission

ABSTRACT

We report the characteristics of heat transfer and emissions in natural gas fired flameless oxidation conditions created using multiple semi-industrial regenerative burners. Burner positions and firing modes (parallel and staggered) are varied, and their effects on efficiency, emissions (NO, CO) and temperature uniformity are studied. Also the excess air ratio and the cycle time have been varied. The operation uses two burner pairs together to provide 200 kW_{th} giving a volumetric heat release closely resembling real industrial operating conditions (48 MW/m^3). The parallel mode operation shows better results concerning low emission of CO and NO, and uniform temperature distribution in the furnace. On the other hand, the staggered mode operation showed a comparatively low performance due to a developed unsymmetrical flow pattern in the furnace. Single digit NO emission was measured for the parallel mode with low CO concentration due to low and uniform temperature. CO concentration is strongly dependent on the burner cycle time because the switching of burners generates periods of unstable and non-uniform flow pattern and also temperature distribution temporarily. The numerical simulation with skeletal reaction showed typical reaction characteristics of flameless oxidation, which is a slow and uniform reaction progress in the furnace. Meanwhile, the reaction model needs to improve its accuracy because the reaction speed appears to be slower than the experiment, and the simulation of a case showed extinguished reaction. The comparable simulation results also showed an order higher CO emission and an order lower NO emission, which is assumed to be related with low reaction kinetics.

1. Introduction

Energy efficiency and emission reduction are two main issues in combustion. The control of nitrogen oxides (NO_x) is also still a main issue in combustion because it plays a key role in acid rain and photochemical smog formation [1]. Dilution of oxidizer or fuel with flue gas [2] and ultra-lean premixed combustion [3] were applied to lower flame temperature in order to suppress thermal NO_x formation. However, these techniques are faced with flame instability when using a high level of dilution or ultra-lean combustion. Flameless Oxidation (FLOX™) [4], also known as High Temperature Air Combustion (HiTAC) [5], or MILD combustion [6], is a technology capable of accomplishing high efficiency and low emissions without flame instability phenomena. It uses delayed mixing of fuel and oxidizer combined with high level of dilution by flue gas via internal recirculation in the main reaction zone. The high momentum injection of the separate fuel and oxidizer flows drives the entrainment of flue gas, thus decreasing the oxygen concentration in the combustion zone. This leads to a more distributed heat release by chemical reaction, avoiding high peak

* Corresponding author at: School of Mechanical Engineering, Kookmin University, Seoul 136-701, South Korea. Tel.: +82 10 4346 6723; fax: +82 2 910 4839.
E-mail address: d.shin@kookmin.ac.kr (D. Shin).

0306-2619/$ - see front matter © 2013 Elsevier Ltd. All rights reserved.
http://dx.doi.org/10.1016/j.apenergy.2013.01.035

temperatures (hot spots) and reducing the thermal NO_x formation [7]. Combined with high preheat temperature of the combustion air, this combustion technique also achieves a high efficiency. The technology of flameless combustion is currently finding gradually more widespread use, e.g. also in gas turbine application [8].

In the earlier studies, flameless oxidation has been investigated in small furnaces to evaluate the characteristics of the turbulent flame structure using laser measurement techniques, such as Laser Induced Fluorescence [9]. Szegö et al. tested a 20 kW_{th} single MILD combustion burner to evaluate the stability criteria and visualize the flame. They also made a simulation of the furnace using the Perfectly Stirred Reactor (PSR) model [10]. A 200 kW_{th} multi-burner HiTAC furnace has been studied at KTH (Kungliga Tekniska Högskolan), Sweden [11,12]. The furnace was operated using two pairs of NFK-HRS-DF regenerative burners, varying the firing mode (parallel, staggered and counter firing). At TU Delft both experimental [13,14] and computational [15] studies were made of a flameless oxidation furnace operating at 300 kW_{th} using three pairs of regenerative burners. The most original feature of this furnace is that it allows for the use of many different burner arrangements, with different distances between the burners and the cooling tubes. This makes it possible to understand the basics of the interplay between the flow fields and reaction zones induced by different burner configurations. However, the previous flow fields in the furnace were limited to be symmetric and the distances between the burners were close so that the effect of the configuration of burner could not be fully investigated. Furthermore, the previously applied thermal load (300 kW_{th}) was too high so that a furnace temperature lower than 1050 °C could not be achieved. Further research at lower thermal load and the effects of asymmetric flow patterns were needed to understand and to derive appropriate design rules for the flameless oxidation furnace. The previous numerical simulation results [15] showed overall effects of the flow field due to the burner configurations, however, the details of the chemical reaction in the flameless oxidation furnace were not fully described.

In the present study, the operation condition is changed to 200 kW_{th} with two pairs of regenerative burners, which enables simpler burner configurations of the parallel or the staggered type, and can allow operation at lower temperatures in the range of 953–1076 °C by the existing cooling tube heat extraction. An asymmetric flow pattern was also investigated by using a staggered burner configuration. The effect of burner configuration and furnace temperature was experimentally investigated with emphasis on study of CO and NO_x emissions. A sample numerical simulation is described to explain how the chemical reaction is estimated by using the simplified Smooke et al. reaction kinetics model [16,17] and to understand the flameless oxidation phenomena in the furnace. Furthermore, the experimental results of furnace temperature, CO and NO concentration of comparable two cases are compared with the simulation results to discuss the accuracy of the reaction model.

2. Experimental setup

Fig. 1 shows a schematic diagram of the multi-burner furnace, which is in operation with two burner pairs. The thermal power is 100 kW_{th} per burner pair. The test series aims at experimentally studying the influence of burner pair configurations, firing modes (parallel, staggered) and operation temperature on emissions of NO and CO.

During the furnace operation two burners are firing simultaneously, while the other two burners are regenerating heat from the flue gas. During regeneration the sucked flue gas traverses the ceramic honeycomb heat absorbers in the burners, while during firing mode the cold combustion air is heated up by the honeycombs. After a preset time interval, i.e. the cycle time, the burners switch from firing to regenerating mode, or vice versa. The fuel used was Dutch Natural Gas (DNG, LHV 31.67 MJ/m^3) which consists of CH_4 81.3%, N_2 14.35%, C_2H_6 2.85%, CO_2 0.89% and 0.61% of some other small concentrations of higher hydrocarbon and inert species (volume basis).

The furnace has inner dimensions of 1500 × 1500 × 1850 mm (length × width × height). The insulation consists of three layers of ceramic bricks of 100 mm thickness each, together 300 mm thick. During the experiments, the temperature in the furnace was measured at various locations with S-type thermocouples. One of those thermocouples, installed in the middle of one sidewall of the furnace, was used to characterize the furnace temperature. Also, the temperature of the preheated air (regenerator temperature) was measured in two burners (one burner pair). The flow rates of fuel and combustion air were measured using orifice plate differential pressure meters (Kalinsky Sensor Elektronik, DS2). Manual valves were used to control the flow rate of combustion air, allowing variation of the exhaust gas O_2 concentration (excess air ratio).

Around 80% of the flue gas is sucked by a fan via the air nozzles over ceramic honeycombs of the regenerating burners, while the remaining flue gas leaves the furnace directly via the central stack at the roof of the furnace. Because the suction flow rate is practically constant, a change in excess air ratio implies a change in the ratio between both exhausts. A cooling system consisting of eight horizontal single ended concentric tubes, four placed close to the bottom of the furnace and four close to the top is applied to control overall furnace temperature as shown in Fig. 1. Air enters the inner tube, turns at the end and flows back through the annulus.

An NDIR gas analyzer set (Sick, MAIHAK S710) monitors the flue gas composition downstream of the regeneration suction fan to detect NO and CO concentrations. In the same position the O_2 concentration is detected using an on-line analyzer based on the paramagnetic method. Every second all the data are stored.

Total amount of 18 flanges for the burners are divided over two opposite sides of the furnace (nine for each wall) and three levels at each wall side (1st, 2nd and 3rd from the bottom), so, it is possible to investigate different burner configurations in the furnace. Among various configurations, two different burner configurations I (C-I) and II (C-II), show in Fig. 2, have been selected and investigated. Burner were positioned the 1st and 2nd level for C-I or 1st and 3rd level for C-II. Also, each of these configurations is operated with two different firing modes (parallel, staggered). Investigation of these different configurations and firing modes could elucidate the effect of burner distance between firing and regenerating burners on efficiency and emissions.

In Fig. 2, the large circles represent the burner flanges, whereas the small circles represent the location of the cooling tubes. Two burners are firing, while the other two burners are regenerating. The [1]red circles represent the firing burners and the blue circles (meshed) represent the regenerating burners. In the unused burner flanges (blank circles) thermocouples have been installed. Two burners fire from the same side wall in a parallel mode operation, while one burner of a pair fires at one side and the other at the opposing side in a staggered mode. After a certain time interval (cycle time), all burners switch and the firing burners start regenerating and vice versa.

The burners are REGEMAT CD 200 B regenerative flameless oxidation burners manufactured by WS Wärmeprozesstechnik GmbH.

[1] For interpretation of color in Fig. 2, the reader is referred to the web version of this article.

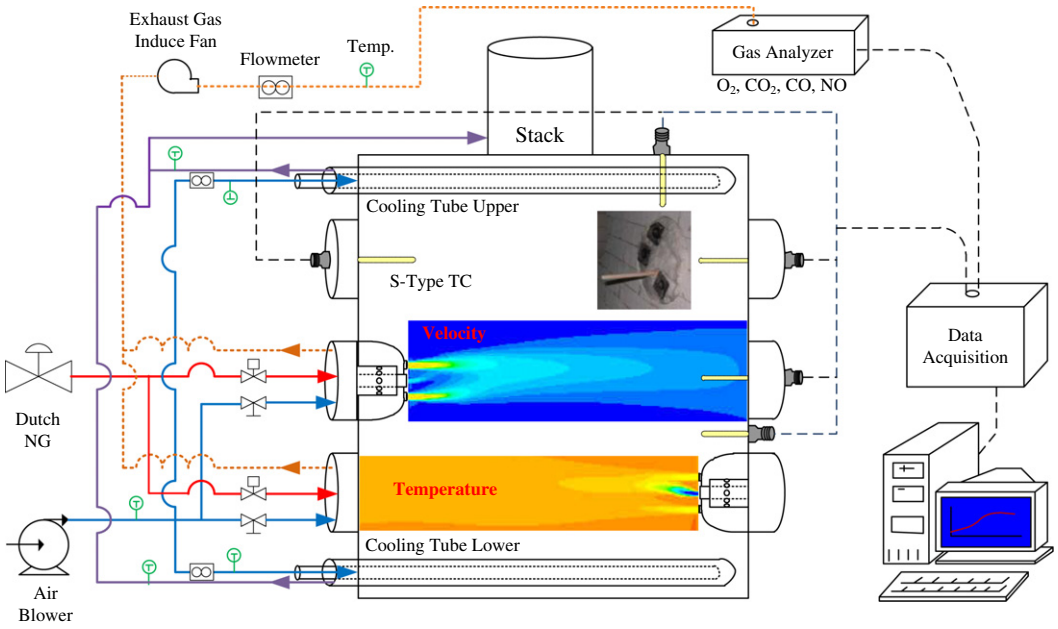

Fig. 1. Schematic diagram of regenerative flameless oxidation furnace.

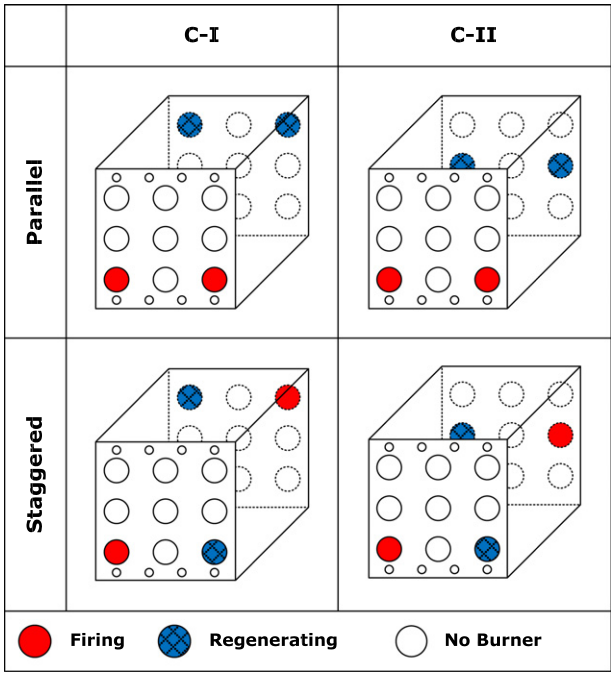

Fig. 2. Multi-burner installation map for the definition of configurations and firing modes.

Each burner has four combustion air nozzles (ϕ = 20 mm) situated around a central fuel nozzle (ϕ = 12 mm). They can operate in two different modes such as flame and flameless condition. In flame mode, the air and fuel are premixed and the mixture is injected through the four air nozzles only, meanwhile the combustion air is injected through the air nozzles and the fuel is injected separately through the fuel nozzle under flameless combustion conditions. The burners fire in flame mode during heating up of the furnace. Once the furnace temperature exceeds 850 °C (this temperature is above the auto-ignition temperature of the natural gas fuel/air mixture), the burners switch to flameless mode automatically. The fuel velocity is 30 m/s (fuel temperature is 25 °C) and the combustion air velocity is around 100 m/s (combustion air is preheated to around 950 °C). Both jets are diluted by flue gas before they meet, and the mixture self-ignites. The reactions take place at locally low O_2 concentrations, which decreases maximum flame temperatures and thus decreases thermal NO_x emission.

3. Numerical method

To simulate the flow and reaction characteristics in the flameless oxidation furnace, a commercial code (FLUENT V. 6.3) is applied. According to the previous study [16] on flameless oxidation simulations, realizable k–ε model for turbulence, EDC (eddy dissipation concept) model based on 46 chemical reactions of the skeletal mechanism and 19 species encountered to simulate natural gas oxidation and NO formation [17], and discrete ordinate model with WSGGM (weighed sum of gray gases model) for radiative heat transfer are adopted. The NO_x has been simulated in postprocessing mode. Because the nitrogen element is not part of the fuel, the fuel NO is not used. The thermal NO which is based upon the instantaneous O and OH, the prompt NO, and the N_2O intermediate which is based upon the transported-simple model are adopted to simulate NO emission along with Smooke reaction mechanism [17,18].

Fig. 3 shows the geometry and computational grid system of 1,046,049 nodes. For simplicity and economics of numerical iteration for parallel firing cases which have symmetric flow pattern, the computational domain covers only half of the furnace and is bounded by a symmetric plane. The wall and cooling tube boundary conditions are selected to fulfill the experimental result of heat transfer at the walls and cooling tubes by calculating heat and mass balance as shown in the previous work [14]. The details of the boundary conditions appear at Table 1.

4. Results and discussion

4.1. Cooling air effects – furnace temperature

Furnace temperature can be controlled by the cooling air flowrate. The furnace temperature was varied from 1076 to 953 °C to

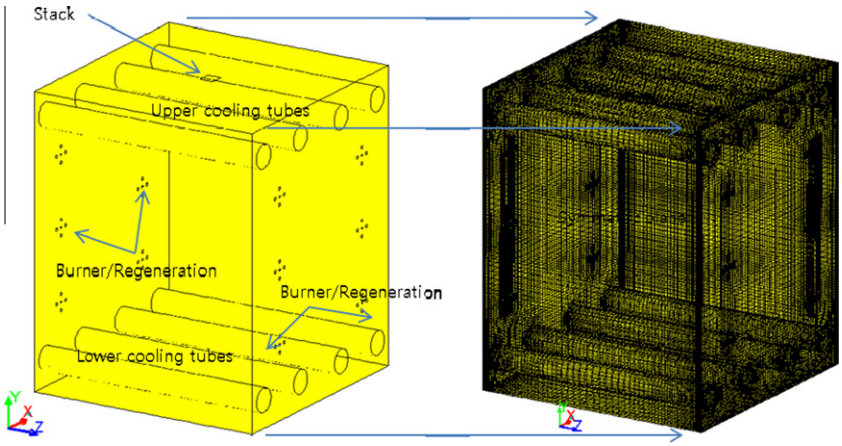

Fig. 3. Geometry of the furnace and the computational grid.

Table 1
Boundary conditions for the CFD simulation.

		Fuel	Air	Regeneration exit	Wall	Cooling tube
Mass flow rate (kg/s)		0.0054	0.094	−0.0668		
Temperature (K)		300	1040		298	298
Species mass fraction	CH_4	0.7598	0			
	CO_2	0.0214	0.0004			
	O_2	0.0002	0.2243			
	H_2O		0.0349			
Heat transfer coeff. (W/m^2 K)					10	20
External emissivity					0.8	–
Wall conductivity (W/m K)					2.25	16.27
Wall thickness (m)					0.3	0.003

investigate the effects of the furnace temperature on emission of NO. Fig. 4a shows the increase of cooling tube heat extraction with increasing cooling air flow rate, and resulting furnace temperature and NO emission. The heat extraction by the upper cooling tubes is always larger than that of the lower tubes, even though they use the same cooling air flow rate. This better heat transfer by the upper tubes is partly due to convection effects (buoyancy and the effect of the flue gas outlet near the upper tubes). Fig. 4b shows that higher heat extraction goes along with lower furnace temperature and lower NO emission. The steady state furnace average temperature decreases from 1076 to 953 °C by increasing the cooling air flow rate, and this decreased temperature results in decrease of NO emission from 15.7 ppm to 5.3 ppm (normalized at 3% O_2).

Fig. 5 shows an overview of the obtained cooling tube efficiency during parallel and staggered mode also with varying cycle times. Cooling tube efficiency is defined as heat extracted by the cooling tubes expressed as percentage of combustion heat input (LHV basis). Cooling tube efficiency decreases with increasing exhaust gas O_2 (higher excess air ratio) due to the decrease in furnace temperature and an increase in flue gas loss.

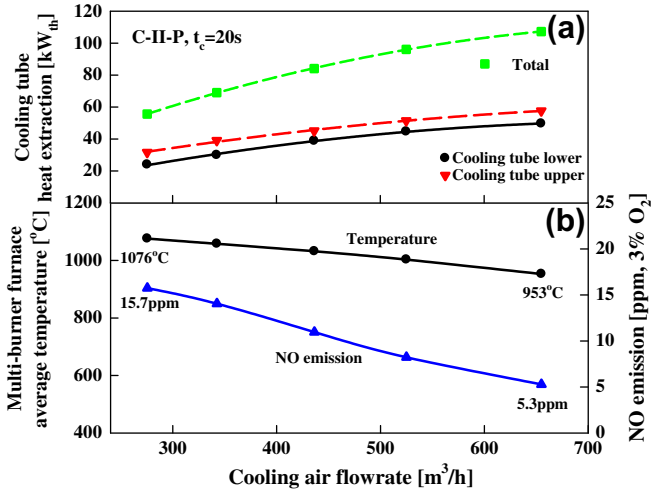

Fig. 4. Cooling tube heat extraction and experimental results of temperature and NO emission as a function of cooling air flow rate.

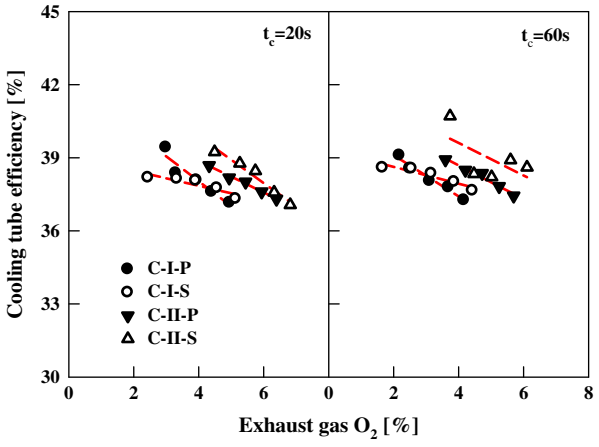

Fig. 5. Trends of cooling tube efficiencies as a function of exhaust gas O_2 (%) for all configurations and cycle times.

At the same exhaust gas O_2 concentration, the C-II configuration shows a slightly higher cooling tube efficiency than C-I. This can be explained by the fact that the furnace temperature of C-II is also higher, enhancing radiative heat transfer (see Fig. 6). In the C-II cases, the staggered mode shows slightly higher cooling tube efficiency than the parallel mode. This is an effect of overall furnace temperature since the staggered mode has slightly lower average temperature (see Fig. 6), which is due to difference in the flow pattern by the different injection points. In general, the choice of cycle time does not have a significant influence on cooling tube efficiency and average temperature.

4.2. Temperature uniformity ratio

Temperature uniformity in the furnace is an important advantage of flameless oxidation. The spatial uniformity of the temperature in the furnace can be characterized by one variable, the temperature uniformity ratio. It is based on the normalized root mean square value computed from all temperature measurements at different locations and is defined as in the following equation.

$$T_u = 1 - \sqrt{\frac{1}{N}\sum_{i=1}^{N}\left(\frac{(T_i - \bar{T})}{\bar{T}}\right)^2} \quad (1)$$

where T_i is the measured temperature at a certain location (i) and $\bar{T}$ is the averaged value of all measured locations in the furnace. The value of T_u is between 0 and 1, where the value 1 indicates a perfectly uniform temperature in the furnace.

Temperatures are measured at 18 different locations in the furnace wall and unused burner flanges using S-type thermocouples. Thermocouples are protruding approximately 100 mm from the inside furnace wall (see Fig. 1).

Fig. 7 shows the spatial furnace temperature uniformity ratio for the considered configurations, firing modes and cycle times. Temperature uniformity ratio increases with higher excess air ratio due to higher jet speed, more turbulence generation and enhanced flue gas recirculation. Also, it is observed that the parallel mode gives a higher temperature uniformity ratio than the staggered mode. In the parallel mode, burners are firing at one side and at the other side burners are regenerating. This leads to a more uniform heating pattern inside the furnace. On the contrary, in the staggered mode, the simultaneously firing burners are located on both sides in a relative position such that an overall swirling flow pattern is generated in the furnace. Thus the flow and reaction patterns are more complicated which lead to larger temperature fluctuations in the furnace. C-II, of which burners are located at low and middle parts of the furnace, shows low temperature uniformity due to intense reaction in the lower part of the furnace. Meanwhile, C-I, of which burners are distributed over low and high parts of the furnace, has more uniform temperature distribution due to even reaction distribution. Hence, the distance between the burners in the furnace is an important parameter to control the furnace performance, and locating the burners at a large enough distance for evenly distributed reaction in the furnace is necessary.

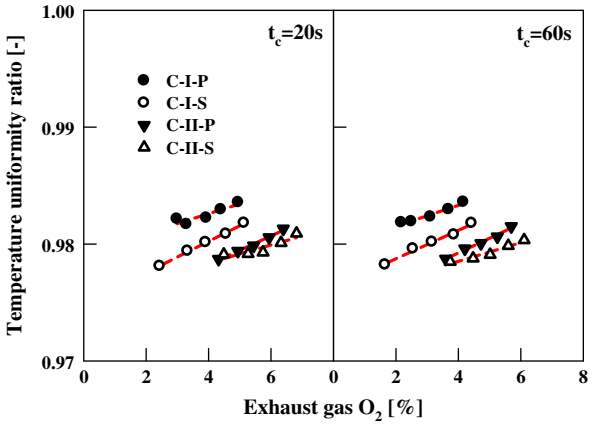

Fig. 7. Trends of furnace temperature uniformity ratio as a function of exhaust gas O_2 (%) for all configurations and cycle times.

4.3. Emissions

Fig. 8 shows the measured NO emissions, which are below 5 ppm normalized at 3% O_2 for parallel modes, and in the range of 5–11 ppm for staggered modes. The reason of higher NO emission of the staggered mode is a complex flow pattern in the furnace which shows spatially concentrated reaction and uneven temperature as shown in Fig. 7. NO emission is not affected significantly by the burner position of the parallel mode. However, that of the staggered mode is influenced by the burner level. The C-II-S (Staggered) configuration for which the burners are located at the 1st and 2nd level, can generate an area of intense reaction in the lower part of the furnace. Meanwhile, C-I–S is a configuration with the burners at the level 1 and 3, for which the distance between the burners is larger than in the C-II-S configuration, so that favorable flameless oxidation conditions can occur with slow reaction speed, resulting in a lower NO emission than C-II-S. The cycle time did not affect the NO emission.

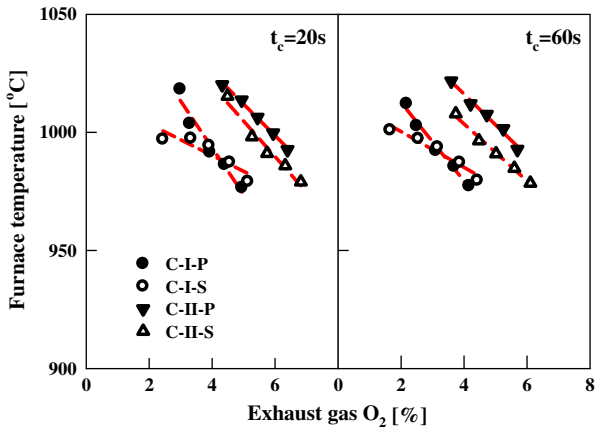

Fig. 6. Trends of furnace temperature as a function of exhaust gas O_2 (%) for all configurations and cycle times.

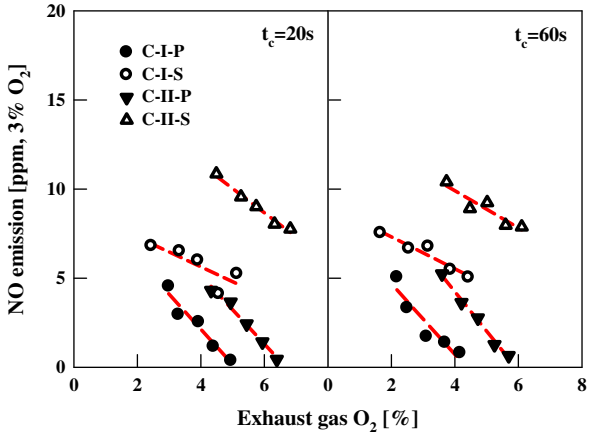

Fig. 8. Trends of NO emission as a function of exhaust gas O_2 (%) for all configurations and cycle times.

Fig. 9 shows the measured time averaged CO emissions. First of all, cycle time has a quite substantial effect on CO emissions and larger cycle time shows lower CO emission. This is explained by the fact that a peak in CO production occurs at the moment of switching of the burners between firing and regeneration. Longer cycle time implies less frequent occurrence of this CO peak, which thus results in overall lower CO emissions. Furthermore, the C-I configuration shows lower CO emissions than C-II. In C-I, the distance between firing and regenerating burners is larger, hence the breakthrough time is also longer. This allows for a higher conversion of CO to CO_2 in the furnace. All the observed CO concentration values in the flue gas are below 40 ppm (normalized at 3% O_2), which is a relatively low value compared to other types of industrial burners.

Regarding the furnace temperature effect on the emission, Fig. 10 shows that the NO emission is directly related with the furnace temperature: as the temperature increases, the NO emission increases. Meanwhile, the firing mode is also a relevant parameter. The parallel modes show better performance with below 5 ppm NO concentration value. The CO emission shown in Fig. 11 also increases as the furnace temperature increases, which shows that flameless oxidation has the benefit of reducing both NO and CO simultaneously. The effect of configuration (I or II) is stronger than the firing mode (P or S), and C-I shows lower CO emission than C-II.

This kind of advantage is also related with temperature uniformity. Theoretically, the furnace temperature is a main parameter determining emissions. However, a case of lower temperature uniformity can be associated with a larger high temperature zone than a higher uniformity case at the same average temperature so that the emission of CO and NO_x can be influenced significantly. As shown in Figs. 12 and 13, the emissions of CO and NO decrease as the temperature uniformity increases, and the band widths of

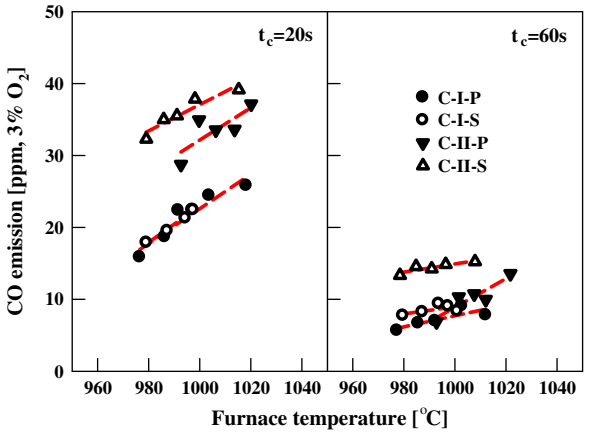

Fig. 11. Trend of CO emission as a function of furnace temperature for all configurations and cycle times.

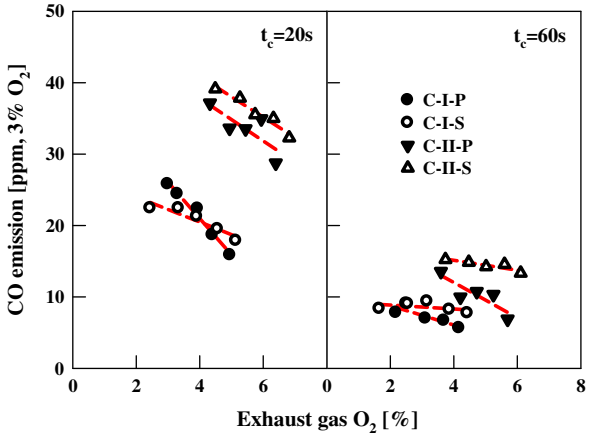

Fig. 9. Trend of CO emission as a function of exhaust gas O_2 (%) for all configurations and cycle times.

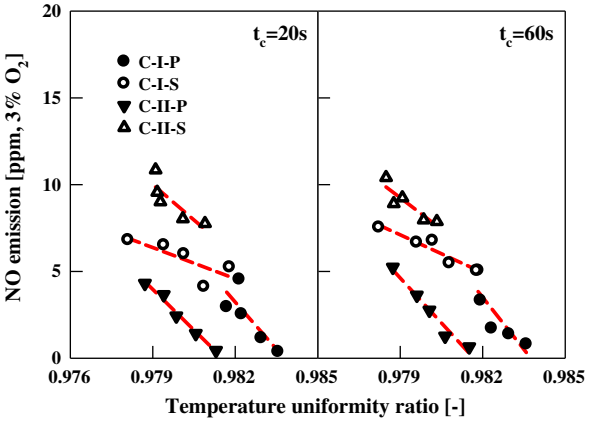

Fig. 12. Trends of NO emission as a function of temperature uniformity ratio for all configurations and cycle times.

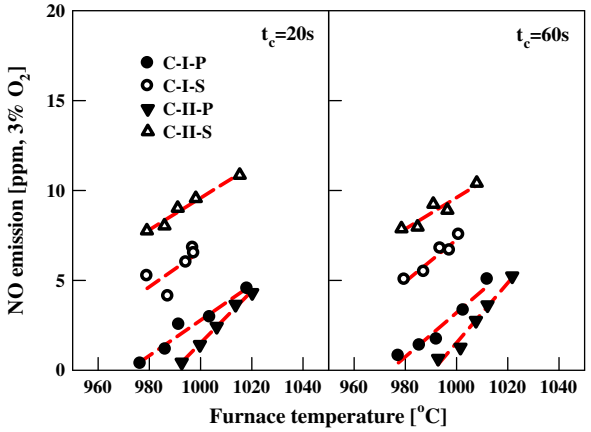

Fig. 10. Trends of NO emission as a function of furnace temperature for all configurations and cycle times.

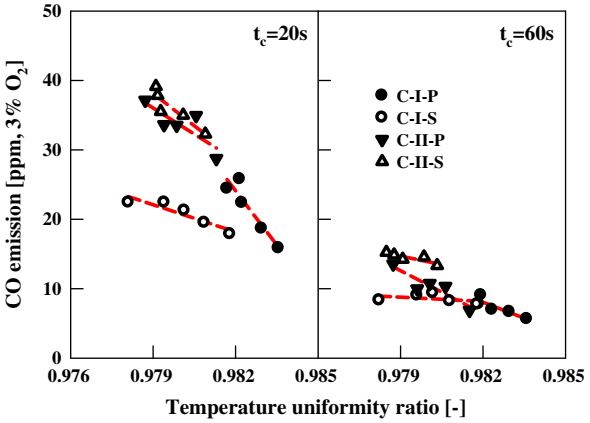

Fig. 13. Trends of CO emission as a function of temperature uniformity ratio for all configurations and cycle times.

the spread data are relatively smaller than shown in Figs. 10 and 11. Hence, temperature uniformity in the furnace can be considered as an important parameter along with average furnace temperature for the flameless oxidation furnace.

4.4. Flow field characteristics by computational fluid dynamics

Fig. 14 shows the calculated velocity vectors in the furnace of C-II-P (Parallel) during steady operation away from burner switching event. In front of the jet nozzles of fuel and air of the burner appears a long jet reaching the opposite wall. After collision with the opposite wall, the jet spreads along the wall in a curbing form and is reflected into the furnace space with low momentum, and eventually sucked into the regenerating burners and the stack. The OH radical concentration shown in Fig. 15, which is a typical indicator of flame or vigorously reacting area, has very low value in the nozzle jet area showing that the model predict that radical reactions or flame do not exist in front of the burner. Meanwhile, high concentration field of OH radical appears at the top and the bottom spaces of the furnace where the burner jet loses its momentum with the oxidation reactions proceeding gradually. OH exists all over the furnace space except the jet area in front and the opposite wall side of the burner, which means a distributed oxidation is generated. CH_3 radical concentration shown in Fig. 16, being the first stage product of CH_4 degradation and a good representative of the initially reacting fuel species, shows an inverse distribution compared to OH. The existence of CH_3 means un-finished reaction and existence of combustible species. Meanwhile, CH_3 radicals disappear where OH radicals are formed due

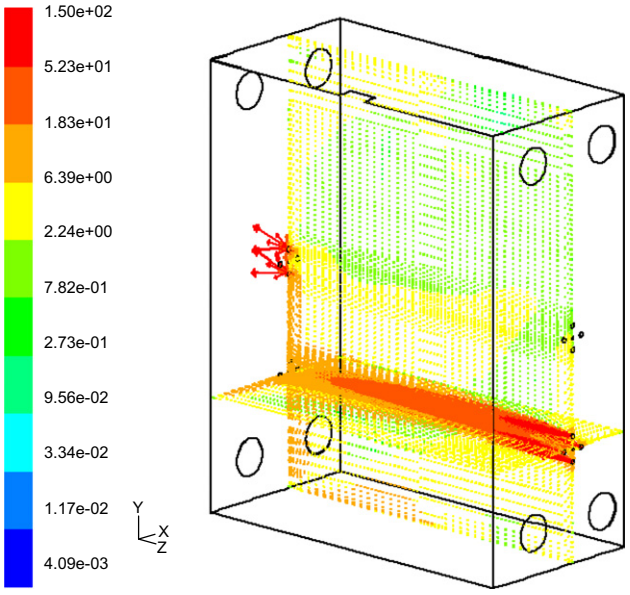

Fig. 14. Result of computational fluid dynamic simulation – velocity vector (m/s).

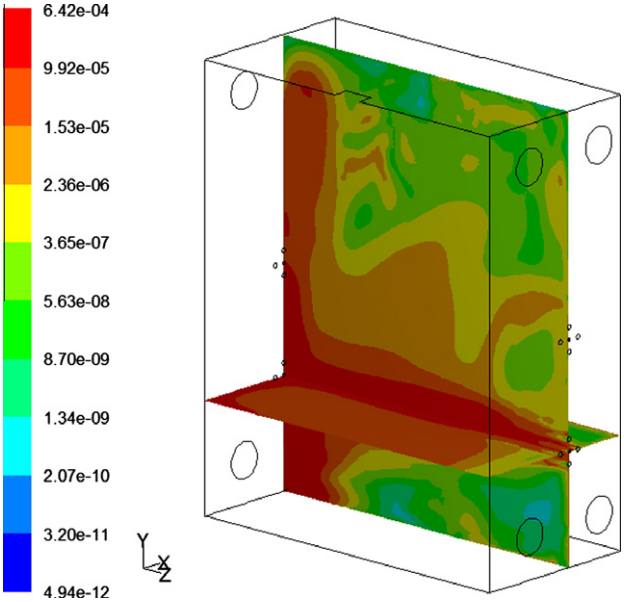

Fig. 16. Result of computational fluid dynamic simulation – CH_3 mole fraction contour.

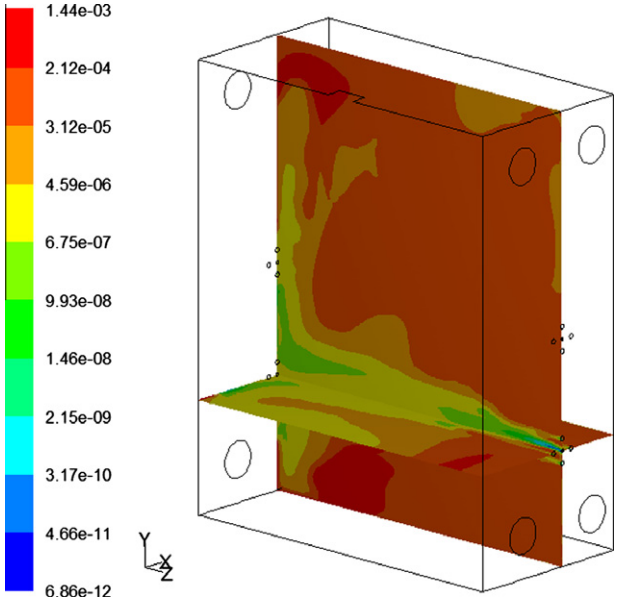

Fig. 15. Result of computational fluid dynamic simulation – OH radical mole fraction contour.

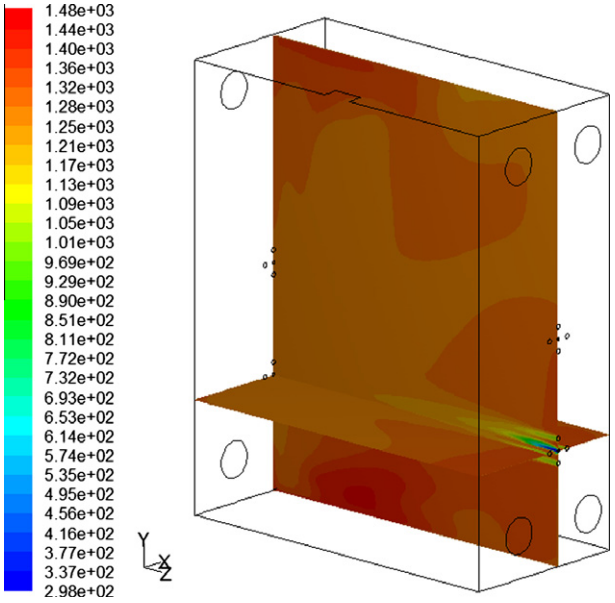

Fig. 17. Result of computational fluid dynamic simulation – temperature contour (K).

Table 2
Comparison of simulation and experimental results for C-II configuration.

	C-II-S		C-II-P	
	Exp.	CFD	Exp.	CFD
Furnace average temperature (K)	1293	1314	1.291	1.295
CO (ppm, 3% O_2)	37.2	265	39.1	384
NO (ppm, 3% O_2)	4.31	0.35	10.8	0.70

to the relatively high reaction rate, and it is converted into the later stage fuel species such as CH_2O and HCO [17]. The temperature distribution in Fig. 17 showing high temperature at the top and the bottom area of the furnace represents these phenomena because the area of high OH concentration is coincident with the high temperature area.

The simulations for experimental cases had been performed, and analyzed to find out the reaction of C-I configuration had been cooled down, which are different from the experimental results. Table 2 summarizes comparison of the C-II-S and C-II-P, which had comparable simulation results. Although the average temperature showed good agreement, the CO concentration is an order higher and the NO concentration is under-estimated at the simulations. The reason of this result is assumed that the reaction model under-estimate the oxidation kinetics, so that the unburned CO concentration is high and special cases like C-I configuration cooled down because of one burner is close to the stack and the distance between the burner and the regeneration exit is relatively far. As NO emission has inversed characteristics of CO, an order lower NO emission result also supports the assumption of low reaction kinetics. Hence, an evaluation study on the reaction kinetics for this kind of scaled-up furnace is recommended as further study.

5. Concluding remarks

The trends in efficiency and emissions of a multi-burner flameless oxidation furnace have been revealed. Operation using two pairs of regenerative burners providing 200 kW_{th} has been studied for two different burner configurations and two different firing modes. A clear conclusion can be drawn concerning the preferred firing mode: parallel firing mode performs better than staggered firing mode, because it shows high temperature uniformity and low emissions of NO and CO for all conditions. C-II has two pair of burners at the low and middle height position of the furnace, so that more intense reactions in the lower part of the furnace are expected. This is the reason why the temperature uniformity of C-II is lower than C-I, and eventually, higher CO and NO emissions are detected. Cycle time of burner operation change has a strong effect on CO emissions. A longer cycle time (60 s) produces lower CO emission levels because the production is localised in time at the switching events. Minimum CO emission is detected at C-I–P to be under 10 ppm. Considering all experiments, it can be concluded that the level of the NO emissions mainly depends on furnace temperature. When the furnace temperature is below 1025 °C, the NO emission is always below 5 ppm (3% O_2) in parallel firing modes. The numerical simulation shows a reasonable explanation of flameless oxidation phenomena in the furnace. While jets from the nozzles of fuel and air penetrate the furnace, mixing of fuel and air occur without real ignition taking place. Meanwhile, after collision with the opposite wall, the jets lose its momentum, reflected and spread in the furnace space, to react evenly in the space, which is generally expected to occur during flameless oxidation. Meanwhile, the reaction kinetics of Smooke model appeared to under-estimate the reaction than the experimental result, which showed an order higher CO and an order lower NO emission. Furthermore, special cases like C-I configuration had been cooled down due to insufficient reaction. Hence, a further study on the reaction kinetics for the scaled-up furnace is recommended.

Acknowledgements

This work is financially supported by the Technology Foundation STW (No. 10428, project of flexFLOX) (The Netherlands), the Industrial Strategy Technology Development (No. 10033389, Development of e-FERA Technology) by the Ministry of Knowledge Economy and research program 2011 of Kookmin Univ. (S. Korea).

References

[1] Baukal CE, Schwartz RE, editors. The John Zink combustion handbook. CRC Press; 2001.
[2] Cho E-S, Chung SH. Characteristics of NO_x emission with flue gas dilution in air and fuel sides. J Mech Sci Technol 2004;18:2303–9.
[3] Cho E-S, Chung SH. Improvement of flame stability and NO_x reduction in hydrogen-added ultra lean premixed combustion. J Mech Sci Technol 2009;23:650–8.
[4] Wünning JA, Wünning JG. Flameless oxidation to reduce thermal NO-formation. Prog Energy Combust Sci 1997;23:81–94.
[5] Tsuji H, Gupta AK, Hasegawa T, Katsuki M, Kishimoto K, Morita M. High temp air combust. CRC Press; 2003.
[6] Cavaliere A, de Joannon M. Mild combustion. Prog Energy Combust Sci 2004;30:329–66.
[7] Miller JA, Bowman CT. Mechanism and modeling of nitrogen chemistry in combustion. Prog Energy Combust Sci 1989;15:287–338.
[8] Arghode VK, Gupta AK. Development of high intensity CDC combustion for gas turbine engines. Appl Energy 2011;88:963–73.
[9] Kobayashi H, Oono K, Cho E-S, Hagiwara H, Ogami Y, Niioka T. Effects of turbulence on flame structure and NO_x emission of turbulent jet non-premixed flames in high-temperature air combustion. JSME Int J 2006;48:286–92.
[10] Szegö GG, Dally BB, Nathan GJ. Operational characteristics of parallel jet MILD combustion burner system. Combust Flame 2009;156:429–38.
[11] Rafidi N, Blasiak W. Heat transfer characteristics of HiTAC heating furnace using regenerative burners. Appl Therm Eng 2006;26:2027–34.
[12] Danon B, Swiderski A, de Jong W, Yang W, Roekaerts DJEM. Emission and efficiency comparison of different firing modes in a furnace with four HiTAC burners. Combust Sci Technol 2011;183:686–703.
[13] Danon B, Cho E-S, de Jong W, Roekaerts DJEM. Parametric optimization study of a multi-burner flameless combustion furnace. Appl Therm Eng 2011;31:3000–8.
[14] Cho E-S, Danon B, de Jong W, Roekaerts DJEM. Behavior of a 300 kW_{th} regenerative multi-burner flameless oxidation furnace. Appl Energy 2011;88:4952–9.
[15] Danon B, Cho E-S, de Jong W, Roekaerts DJEM. Numerical investigation of burner configuration effects in a multi-burner flameless combustion furnace. Appl Therm Eng 2011;31:3885–96.
[16] De A, Oldenhof E, Sathiah P, Roekaerts DJEM. Numerical simulation of Delft-Jet-in-Hot-Coflow (DJHC) flames using the Eddy dissipation concept model for turbulence–chemistry interaction. Flow Turb Combust 2011;87:537–67.
[17] Smooke MD, Puri IK, Seshadri K. A comparison between numerical calculations and experimental measurements of the structure of a counterflow diffusion flame burning diluted methane in diluted air. Proc Combust Inst 1986;21:1783–92.
[18] Fluent user guide V 6.3; FLUENT, Inc.; 2006.